Tetrahedron 67 (2011) 8383–8391

Contents lists available at SciVerse ScienceDirect

Tetrahedron

journal homepage: www.elsevier.com/locate/tet

1,3-Dipolar cycloaddition of 1*H*-pyrazinium-3-olate and *N*1- and *C*-methyl substituted pyrazinium-3-olates with methyl acrylate: a density functional theory study

Lydia Rhyman [a], Hassan H. Abdallah [b], Sabina Jhaumeer-Laulloo [a], Luis R. Domingo [c], John A. Joule [d], Ponnadurai Ramasami [a,*]

[a] *Department of Chemistry, University of Mauritius, Réduit, Mauritius*
[b] *School of Chemical Sciences, Universiti Sains Malaysia, 11800 Penang, Malaysia*
[c] *Departamento de Química Orgánica, Universidad de Valencia, Dr. Moliner 50, 46100 Burjassot, Valencia, Spain*
[d] *The School of Chemistry, The University of Manchester, Manchester M13 9PL, UK*

ARTICLE INFO

Article history:
Received 10 May 2011
Received in revised form 25 July 2011
Accepted 8 August 2011
Available online 22 August 2011

ABSTRACT

A DFT study of the 1,3-dipolar cycloaddition of methyl acrylate to 1*H*-pyrazinium-3-olate and *N*1- and *C*-methyl substituted pyrazinium-3-olates, in the gas phase and in THF, has been carried out at the B3LYP/6-31G(d) level. Two stereoisomeric pathways, *endo* and *exo*, and two regioisomeric channels, 2-oxo-3,8-diazabicyclo[3.2.1]octane-6-ester and 7-ester products, have been considered. Thermodynamic and kinetic parameters calculated at room temperature have been analyzed. The regioselectivity has been interpreted using reactivity indices. It is generally found that the *exo* pathway is preferred and the formation of the 6-esters is dominant. The theoretical data obtained for the cycloaddition reaction of 1,5-dimethylpyrazinium-3-olate with methyl acrylate are consistent with the literature where the 6-*exo* regioisomer is formed as the major cycloadduct.

1. Introduction

The 1,3-dipolar cycloaddition (1,3-DC) reaction is an effective route for the synthesis of five-membered heterocyclic structures.[1–10] The ring systems arising from 1,3-DCs are the backbones of some natural products.[11–13] Nitrogen-containing heterocycles occur widely in nature, in isolation and as structural subunits in various families of alkaloids with laboratory,[14–16] industrial and pharmacological applications.[8,17–20] Following on from and inspired by the pioneering studies of Katritzky et al. on pyridinium-3-olates,[21–25] we have been particularly interested in the cycloaddition reactions of pyrazinium-3-olates[26–32] as a means for the construction of complex structures. Apart from synthesis, theoretical methods are becoming increasingly useful to investigate 1,3-DC processes.[33–37]

In a recent report,[38] we carried out a theoretical study on the 1,3-DC of 1*H*-pyridinium-3-olate and 1-methylpyridinium-3-olate with methyl acrylate (**MA**) at the B3LYP/6-31G(d) level of theory. Both the 6-ester/7-ester regioisomeric pathways were taken into consideration so as to have a better insight into the reaction mechanism. The theoretical results obtained were in accord with experimental outcomes showing that 8-azabicyclo[3.2.1]oct-3-en-2-one-6-esters are formed preferentially.[39]

We have previously studied experimentally the cycloadditions of a range of 1-substituted 5-methylpyrazinium-3-olates with unsymmetrical dipolarophiles.[26–32] These reactions produced 4-methylene-2-oxo-3.8-diazabicyclo[3.2.1]octane-6-carboxylates, of interest for the construction of natural products, such as anticancer quinocarcin[40–42] and antibiotic lemonomycin,[43] both of which include this subunit.

We first studied[31] experimentally the cycloaddition of 1,5-dimethylpyrazinium-3-olate (**1b**) with **MA** (Scheme 1—note that in all the experimental work reported to date, the pyrazinium-3-olates have had an alkyl group at C-5, leading, when R^3=Me to an exocyclic methylene product, formed by a simple tautomerism of the initial cycloadduct (**CA**)), and a mixture of the 6-*exo* (**CA6ex**) and 6-*endo* (**CA6en**) isomers in a ratio of 4:1 was observed in both acetonitrile and THF solutions. A minor amount of the 7-*exo* CA (**CA7ex**) was also formed and characterized, however, 7-*endo* isomer was formed when using phenyl vinyl sulfone as the dipolarophile.[27] In enlarging the range of *C*-substituted pyrazinium-3-olates examined,[28–30,32] we extended our experimental investigations by assessing the influence of introducing *C*-methyl and *C*-ethyl substituents at the future ring-junction of the 1,3-dipole. The effect of greater encumbrance was clearly observed as in several of the CAs extensive rearrangement had taken place.

The current computational study extends the scope of the previous research[38] by investigating the 1,3-DC reactions of 1*H*-

* Corresponding author. E-mail address: ramchemi@intnet.mu (P. Ramasami).

0040-4020/$ – see front matter © 2011 Elsevier Ltd. All rights reserved.
doi:10.1016/j.tet.2011.08.021

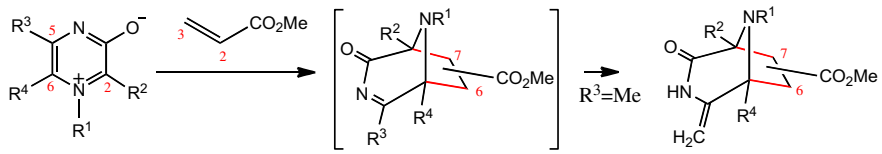

	R^1	R^2	R^3	R^4
1	H	H	H	H
1a	Me	H	H	H
1b	Me	H	Me	H[27,31]
1c	Me	H	H	Me
1d	Me	Me	H	H

Scheme 1. Model substrates for the 1,3-DC of *N*1-substituted and *C*-methyl substituted pyrazinium-3-olates (**1**, **1a**, **1b**, **1c** and **1d**) with **MA**.

pyrazinium-3-olate **1**, and *N*1- and *C*-methyl substituted pyrazinium-3-olates **1a**–**d** with **MA** in the gas phase and in THF as solvent (see Scheme 1). Within this goal stereo- and regioselectivity, thermodynamic and kinetic parameters for the 1,3-DC of pyridinium-3-olates and pyrazinium-3-olates with **MA** are compared and the effect of varying the position of the methyl group in the pyrazinium-3-olate ring is examined in a systematic way. Furthermore, the regio- and stereoselectivity of the reaction between 1,5-dimethylpyrazinium-3-olate **1c** and **MA** are compared with the experimental outcomes.[31]

2. Computational methods

All computations were carried out with the Gaussian 03 suite of programs.[44] The full geometry optimizations of all structures and transition state structures (TSs) were computed using density functional theory (DFT) by applying the three-parameter hybrid functional by Becke's[45] (B3) and the correlation functional by Lee-Yang-Parr's[46] (LYP). The basis set 6-31G(d)[47] has been employed as it is a well-established method for the prediction of activation energies of cycloaddition reactions and to provide geometries and electronic properties in good correlation with literature.[48–50] Reactants and CAs were characterized by frequency computations and have positive definite Hessian matrices. The TSs had only one negative eigenvalue in their diagonalized force constant matrices. The vibrational mode was assigned appropriately by means of visual inspection and animation using the CYLVIEW program.[51] Furthermore, the intrinsic reaction coordinate (IRC)[52,53] path was traced to authenticate the connection of a TS to the two associated minima of the proposed mechanism. Solvent effects were taken into account with the polarizable continuum model (PCM) as developed by Tomasi's group[54–56] in the framework of self-consistent reaction field (SCRF).[57,58] The solvent used in this present research was THF, with temperature and pressure considered at 298.15 K and 1 atm. The reported electronic energies include zero-point energies (ZPE) corrections scaled by a factor of 0.96.[59] Natural bond orbital (NBO) analysis was performed on the electronic structures of the critical points according to Weinhold et al.[60,61] using NBO 3 as implemented in Gaussian 03.

The global electrophilicity index, ω, is given by the following simple expression,[62] $\omega=(\mu^2/2\eta)$, in terms of the electronic chemical potential μ and the chemical hardness η. Both quantities may be approached in terms of the one electron energies of the frontier molecular orbital HOMO and LUMO, ε_H and ε_L, as $\mu\approx(\varepsilon_H+\varepsilon_L)/2$ and $\eta\approx(\varepsilon_L-\varepsilon_H)$, respectively.[63,64] Recently, we have introduced an empirical (relative) nucleophilicity index, N based on the HOMO energies obtained within the Kohn–Sham scheme,[65] and defined as $N=\varepsilon_{H(Nu)}-\varepsilon_{H(TCE)}$. Tetracyanoethylene (TCE) is chosen as reference as it presents the lowest HOMO energy in a large series of molecules already investigated in the context of polar cycloadditions. This choice allowed us conveniently to handle a nucleophilicity scale of positive values.[66] Local electrophilicity[67] and nucleophilicity[68] indices, ω_k and N_k were evaluated using the following expressions: $\omega_k = \omega f_k^+$ and $N_k = N f_k^-$ where f_k^+ and f_k^- are the Fukui functions for a nucleophilic and electrophilic attacks, respectively.[69]

The rate constant, calculated at 298.15 K, is predicted according to the following equation:

$$\mathbf{1} + \mathbf{2} \underset{k_{-1}}{\overset{k_1}{\rightleftharpoons}} \mathrm{TS} \overset{k_2}{\rightarrow} \mathrm{CA} \tag{1}$$

The effective rate constant corresponding to the formation of CAs can, thus, be calculated as:

$$k_{ef} = \frac{k_1 k_2}{k_{-1} + k_2} \tag{2}$$

The rate constant of each step is calculated based on the conventional transition state theory (TST)[70–72] equations:

$$k_1 = \kappa \frac{k_B T}{h} \frac{\mathrm{RT}}{p} \exp\frac{\Delta S^\circ}{R} \exp\left(-\frac{\Delta H^\circ}{\mathrm{RT}}\right) \tag{3}$$

$$k_{-1} = \kappa \frac{k_B T}{h} \exp\left(-\frac{\Delta S^\circ}{R}\right) \exp\left(\frac{\Delta H^\circ}{\mathrm{RT}}\right) \tag{4}$$

$$k_2 = \kappa \frac{k_B T}{h} \exp\left(\frac{\Delta S^{\neq}}{R}\right) \exp\left(-\frac{\Delta H^{\neq}}{\mathrm{RT}}\right) \tag{5}$$

where k_B is Boltzmann's constant; h is Planck's constant, T is the temperature; R is the ideal gas constant; κ is the transmission coefficient and is taken to be 1; ΔH° is the relative enthalpy, $\Delta H^{\neq}$ is the activation enthalpy while ΔS° and $\Delta S^{\neq}$ are the relative and activation entropies, respectively.

In addition, k_1, has also been calculated with the Wigner tunneling coefficient[70,73] according to the standard Eyring TST as:

$$k_1 = I \frac{k_B T}{h} \frac{Q_{TS} N_A}{Q_1 Q_2} \exp\left(-\frac{\Delta E_a}{\mathrm{RT}}\right) \tag{6}$$

where N_A is the Avogadro's number; Q_{TS}, Q_1, and Q_2 are the total partition functions of TS, **1** and **2**, respectively and ΔE_a is the activation barrier for the cycloaddition. The values of the rate constants are calculated at standard conditions (T=298.15 K and p=101,325 Pa).

3. Results and discussion

3.1. Energetics

3.1.1. 1,3-DC reaction of 1H-pyrazinium-3-olate ***1*** *and 1-methylpyrazinium-3-olate* ***1a****, with methyl acrylate.* The 1,3-DC reactions of 1*H*-pyrazinium-3-olate **1** and 1-methylpyrazinium-3-

olate **1a** with the unsymmetrical dipolarophile, **MA**, can yield four isomeric CAs, the *endo* and *exo* stereoisomers of the two possible regiochemical pathways: 6-substituted CAs involve bond formation between the pyrazinium-3-olate C2 and **MA** C3 carbons and the pyrazinium-3-olate C6 and **MA** C2 carbons, while 7-substituted CAs have the opposite regiochemical orientation. Hence, four TSs, designated **TS6en-1x**, **TS6ex-1x**, **TS7en-1x**, **TS7ex-1x** and the corresponding CAs, **CA6en-1x**, **CA6ex-1x**, **CA7en-1x**, **CA7ex-1x**, where **x** (**x**=**a**, **b**, **c**, **d** or **e**) signifies the substituted pyrazinium taken into consideration, were located and characterized. Note, that along the *endo* channels, the C3, C4, and C5 carbons of the pyrazinium ring overlay the ester group of **MA**, while along the *exo* channels, only the N1 nitrogen could interact with the ester group (Figs. 1 and 2). Table 1 reports the activation energies and reaction enthalpies of the 1,3-DC reactions of the pyrazinium **1** and **1a** with **MA**.

Likewise, for the reaction of 1-methylpyrazinium-3-olate **1a** with **MA**, the *exo* approach remains the more favorable pathway; **TS6ex-1a** and **TS7ex-1a** are lower in energy than **TS6en-1a** and **TS7en-1a** by 8.0 and 7.6 kJ mol^{-1} in THF. Furthermore, this reaction channel favors the same regiochemical sense, 6-esters, as that observed in Katritizky's work on pyridinium-3-olates[21–25] and the previous theoretical[38] outcome of our study of cycloaddition reactions of pyridinium-3-olates with **MA**.

The thermodynamic parameters including activation enthalpies and activation Gibbs free energies as well as the reaction enthalpies and reaction Gibbs free energies computed at 298.15 K and 1 atm in THF are gathered in Table 2. The computed activation enthalpies range from 54.8 to 66.0 kJ mol^{-1} for the 1,3-DC reaction of 1*H*-pyrazinium-3-olate **1**, while a range of 44.2–63.5 kJ mol^{-1} is observed for the 1,3-DC reaction of 1-methylpyrazinium-3-olate **1a**. It

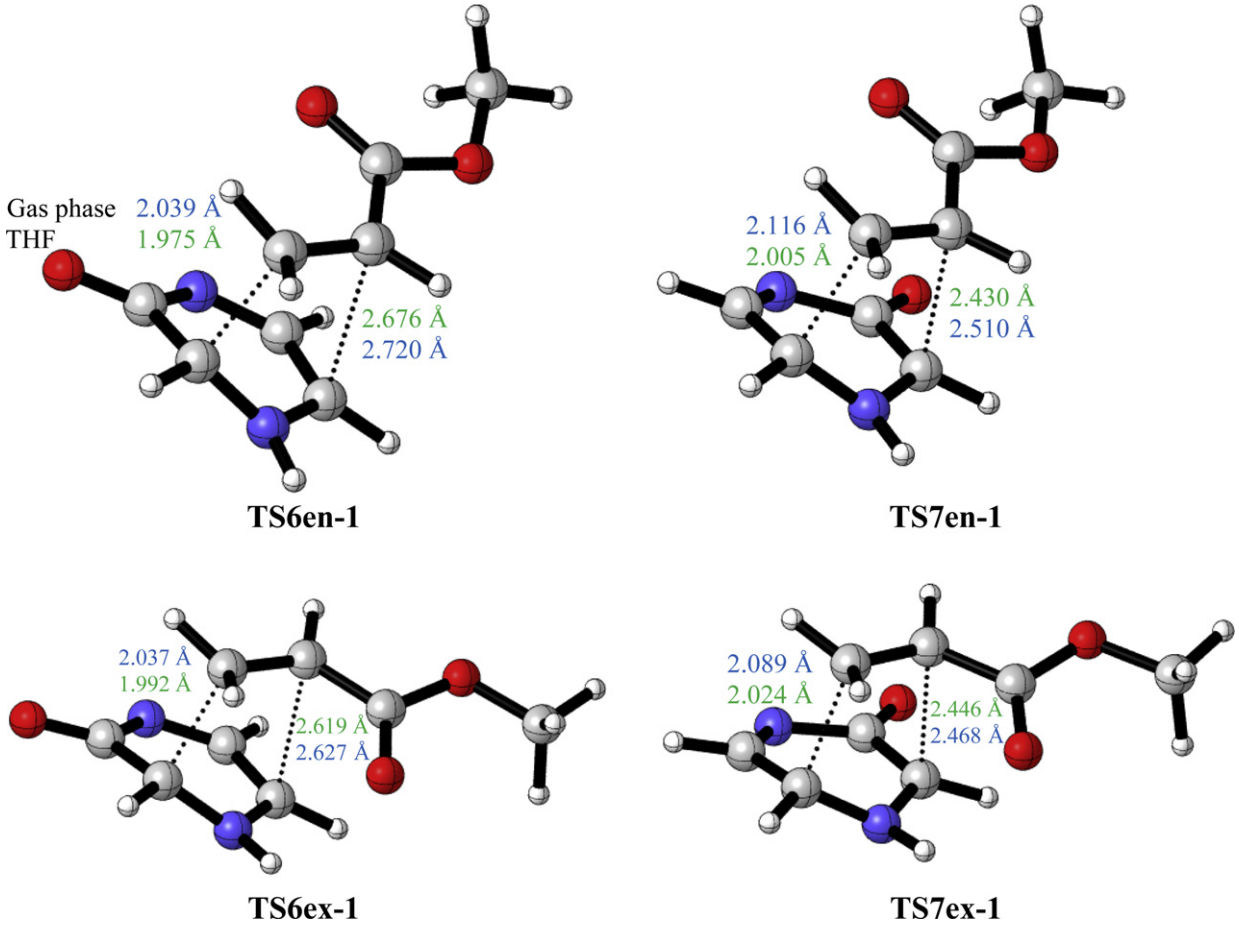

Fig. 1. B3LYP/6-31G(d) optimized geometries of the TSs involved in the 1,3-DC reaction between 1*H*-pyrazinium-3-olate **1** with **MA**.

In the gas phase, the *exo* approach mode is favored over the *endo* one by ca. 28.6 and 24.5 kJ mol^{-1} leading to the 6- and 7-substituted CAs, respectively, for the reaction of pyrazinium-3-olate **1** with **MA**. Similarly, for the reaction of 1-methylpyrazinium-3-olate **1a** with **MA**, the *exo* pathway is more favored over the *endo* pathway by ca. 20.9 kJ mol^{-1} leading to the 6-substituted CAs, and by ca. 14.8 kJ mol^{-1} leading to the 7-substituted CAs. The gas phase energy differences between 6-*exo* and 7-*exo* (9.1 kJ mol^{-1} for **1**+**MA** and 12.0 kJ mol^{-1} for **1a**+**MA**) and between 6-*endo* and 7-*endo* (5.0 kJ mol^{-1} for **1** and 5.9 kJ mol^{-1} for **1a**) are too small to account for the regioselectivity.

In THF, the *exo* approach for the reaction of **1** with **MA** remains favored over the *endo* approach; **TS6ex-1** and **TS7ex-1** are lower in energy than **TS6en-1** and **TS7en-1** by 11.1 and 10.9 kJ mol^{-1}. It is interesting to note that the activation enthalpy for the *exo* approach is lower compared to the *endo* approach for the reaction of 1*H*-pyrazinium-3-olate **1** with **MA**, in line with the calculated activation energy. Moreover, the activation entropy corresponding to the *exo* channel is more negative than that corresponding to the *endo* channel. As a consequence, the activation free energies for formation of the **CA6ex-1** and **CA7ex-1** are lower than those for **CA6en-1** and **CA7en-1**. Similarly, for the reaction of 1-methylpyrazinium-3-olate **1a** with **MA** comparable observations are made for the preferred reaction pathways leading to the formation of 6-esters.

We find that all these 1,3-DCs are exothermic processes (Table 2) and the **CA6ex** is slightly more stable than the **CA6en** (Table 1). Moreover, from kinetic and thermodynamic points of view, the

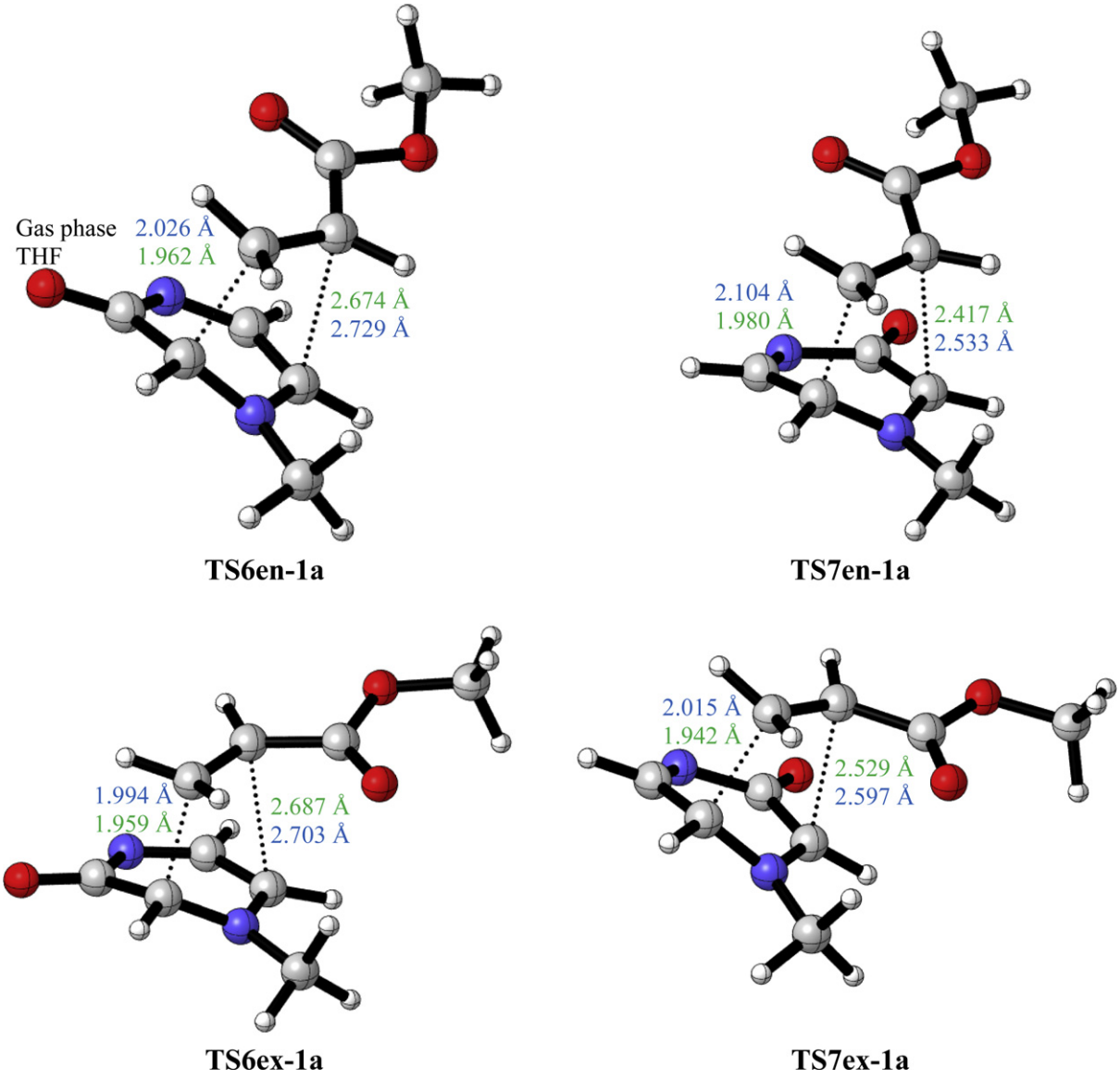

Fig. 2. B3LYP/6-31G(d) optimized geometries of the TSs involved in the 1,3-DC reaction between 1-methylpyrazinium-3-olate **1a** with **MA**.

results show that the pathways leading to the **CA6ex** are always preferred independent of the *N*-substituent. In addition, the expected CAs for the reaction of 1*H*-pyrazinium-3-olate **1** with **MA**, would be a mixture of 6-*exo* and 7-*exo* CAs with 6-*exo* as the major product. The 7-*exo* product would also be formed to the same extent as they are close in energies. However, the 6-*endo* and 7-*endo* CAs might be observed in minor amounts. On the other hand, for the reaction of 1-methylpyrazinium-3-olate **1a** with **MA**, the 6-esters are the dominant CAs where the 6-*exo* is expected to be the major product followed by the 6-*endo*. The other significant product would be the 7-*exo* due to the comparable activation energies to the 6-esters.

3.1.2. Comparison of the 1,3-DC reactions of pyridinium-3-olates and pyrazinium-3-olates with methyl acrylate. The activation energies for the 1,3-DC of **MA** with pyridinium-3-olates are higher than those for the reactions with pyrazinium-3-olates. Additionally, the 6-*exo* TSs are kinetically favored over the 6-*endo* ones in THF, and the decrease in activation energies is larger when the nitrogen (N1) is substituted with a methyl. Furthermore, the relative energies of the CAs increase with the inclusion of the second nitrogen in the pyrazinium ring and thus, the CAs become more stable. In general, a larger relative energy difference is found for the *exo* approach for both systems. From Table 2, it can be seen that the CAs are more exothermic when **MA** reacts with pyrazinium-3-olates. For the 6-esters, the exothermicity difference between the two different systems is larger for the *exo* mode of addition over the *endo* mode while the opposite is observed for the 7-esters. It can also be observed that there is a larger difference in the relative energy and enthalpy with the unsubstituted pyridinium-3-olate and pyrazinium-3-olate compared to 1-methylpyridinium-3-olate and 1-methylpyrazinium-3-olate.

3.1.3. Effects of the methyl substitution on the pyrazinium ring. This section is devoted to the 1,3-DC reactions of **MA** with 1,5-dimethylpyrazinium-3-olate **1b**, 1,6-dimethylpyrazinium-3-olate **1c** and 1,2-dimethylpyrazinium-3-olate **1d**. In the ongoing discussion, the acronyms **1b**, **1c**, and **1d** are added to the TSs and CAs. The energetic parameters of the various pathways of the cycloaddition reactions are listed in Table 3.

The relative energies in THF given in Table 3 indicate that the regiochemical channels leading to the 6-esters are more favorable than the channels leading to the 7-esters for the reaction of **1b** and **1c** with **MA**. The energy differences between the 6-*endo* and 6-*exo*

Table 1
Energies (E, in au) and relative energies[a] (ΔE, in kJ mol^{-1}) computed at 298.15 K and 1 atm in gas phase and THF involved in the 1,3-DC reactions of **1** and **1a** with **MA**

	Gas phase		THF	
	E	ΔE	*E*	ΔE
1	−339.436668	—	−339.456442	—
1a	−378.723995	—	−378.742348	—
MA	−306.374595	—	−306.380500	—
TS6en-1	−645.788739	59.1 (83.3)[b]	−645.810996	68.1 (74.9)[b]
TS6ex-1	−645.799654	30.5 (60.0)	−645.815226	57.0 (67.7)
TS7en-1	−645.786832	64.1 (91.0)	−645.807590	77.1 (86.1)
TS7ex-1	−645.796165	39.6 (70.1)	−645.811746	66.2 (77.2)
TS6en-1a	−685.076601	57.7 (82.9)	−685.102116	54.4 (68.8)
TS6ex-1a	−685.084586	36.8 (70.5)	−685.105172	46.4 (66.5)
TS7en-1a	−685.074383	63.6 (90.6)	−685.097825	65.7 (81.7)
TS7ex-1a	−685.080010	48.8 (80.4)	−685.100701	58.1 (75.5)
CA6en-1	−645.838740	−72.1 (−40.3)	−645.851533	−38.3 (−25.0)
CA6ex-1	−645.839921	−75.2 (−42.0)	−645.852927	−42.0 (−26.7)
CA7en-1	−645.839149	−73.2 (−39.9)	−645.851873	−39.2 (−22.7)
CA7ex-1	−645.839579	−74.3 (−40.4)	−645.852611	−41.1 (−24.8)
CA6en-1a	−685.121688	−60.6 (−29.8)	−685.133441	−27.8 (−25.1)
CA6ex-1a	−685.122976	−64.0 (−26.1)	−685.134833	−31.5 (−21.0)
CA7en-1a	−685.122018	−61.5 (−28.7)	−685.134207	−29.8 (−22.4)
CA7ex-1a	−685.122641	−63.1 (−27.8)	−685.134569	−30.8 (−23.1)

[a] Relative to **1**+**MA** or **1a**+**MA**.
[b] Values in parentheses are the relative energies for the reaction of 1*H*-pyridinium-3-olate and 1-methylpyridinium-3-olate with **MA** (see Ref. 38).

Table 2
Relative enthalpies[a] (ΔH, in kJ mol^{-1}), free energies (ΔG, in kJ mol^{-1}) and entropies (ΔS, in J mol^{-1}) computed at 298.15 K and 1 atm in THF for the TSs and CAs involved in the 1,3-DC reactions of **1** and **1a** with **MA**

	ΔH	ΔG	ΔS		ΔH	ΔG	ΔS
TS6en-1	66.0	122.4	−188.9	**TS6en-1a**	52.4	109.7	−192.3
TS6ex-1	54.8	111.6	−190.5	**TS6ex-1a**	44.2	102.3	−195.1
TS7en-1	75.1	130.4	−185.5	**TS7en-1a**	63.5	121.5	−194.5
TS7ex-1	64.0	120.7	−190.0	**TS7ex-1a**	55.9	114.3	−196.1
CA6en-1	−42.1 (−29.3)[b]	15.6	−193.6	**CA6en-1a**	−31.9 (−27.7)[b]	28.3	−201.9
CA6ex-1	−45.7 (−30.9)	12.5	−195.3	**CA6ex-1a**	−35.6 (−25.2)	25.2	−204.1
CA7en-1	−43.1 (−26.9)	15.6	−196.9	**CA7en-1a**	−43.0 (−24.9)	19.0	−207.8
CA7ex-1	−44.9 (−29.0)	12.4	−192.1	**CA7ex-1a**	−34.9 (−25.6)	25.5	−202.3

[a] Relative to **1**+**MA** or **1a**+**MA**.
[b] Values in parentheses are the relative enthalpies for the reaction of 1*H*-pyridinium-3-olate and 1-methylpyridinium-3-olate with **MA** (see Ref. 38).

Table 3
Relative energies[a] (ΔE, in kJ mol^{-1}) computed at 298.15 K and 1 atm in gas phase and THF involved in the 1,3-DC reactions of **1b**–**d** with **MA**

	1b	**1c**	**1d**
Gas phase			
TS6en	53.7	54.1	67.2
TS6ex	33.3	28.6	46.3
TS7en	58.1	65.5	64.8
TS7ex	43.6	50.7	46.4
CA6en	−68.8	−58.6	−53.5
CA6ex	−73.8	−57.5	−49.1
CA7en	−71.9	−61.3	−53.8
CA7ex	−73.3	−63.5	−49.1
THF			
TS6en	62.6	55.4	76.2
TS6ex	54.8	42.5	67.1
TS7en	72.1	73.1	77.2
TS7ex	63.7	66.3	65.3
CA6en	−37.4	−32.2	−18.8
CA6ex	−40.1	−31.5	−15.1
CA7en	−39.4	−26.4	−18.9
CA7ex	−41.2	−36.2	−15.1

[a] Relative to **1x** (**x**=**b**, **c** and **d**)+**MA**.

are 7.8 and 12.9 kJ mol^{-1} for the reaction of **1b** and **1c** with **MA**, respectively, whereby, the *exo* TSs are kinetically more favorable relative to the *endo* TSs. However, an exception is observed for the reaction of **MA** with **1d** where the channels leading to the *exo* TSs (**TS6ex-1d** and **TS7ex-1d**) have comparable activation energies to the channels leading to the *endo* TSs (**TS6en-1d** and **TS7en-1d**). A difference of only 1.8 kJ mol^{-1} is noted between the two *exo* TSs; **TS7ex-1d** has lower energy than **TS6ex-1d**.

The preferred reaction pathway for the reaction of **1b** with **MA** is the channel leading to the 6-esters, which have lower activation energies (62.6 and 54.8 kJ mol^{-1}) compared to the channels leading to the 7-esters. From a kinetic point of view, it can be concluded that the 6-*exo* pathway is preferred over the 6-*endo* and these results agree with the experimentally observed major product and with the isolation of the 6-esters with a predominating 6-*exo* CA in the ratio 4:1.[26] The next significant CA in the reaction mixture should also consist of the 7-*exo* CA as its corresponding TS has comparable activation energies to the 6-esters. This is in accord with experimental findings where we were able to characterize the presence of a 7-*exo* CA.[27]

The possible outcomes for the reaction of **1c** and **1d** with **MA** are also predicted as these are experimentally untried. The introduction of a methyl substituent at the C6 position on pyrazinium **1c** shows that the 6-*exo* reaction channel remains the most favorable pathway. It can be concluded that both the 6-*exo* and 6-*endo* CAs are expected to be formed kinetically. However, the 6-*endo* product is slightly more stable than the 6-*exo* product. The introduction of a methyl group at C2 on pyrazinium **1d** does not yield the same ordering of CAs formation as with pyraziniums **1b** and **1c**. The 1,3-DC reaction mechanism shows that the predominating CAs are the *exo* esters; 6-*exo* and 7-*exo*. Surprisingly, the 7-*exo* channel is comparable to the 6-*exo* channel. For the reaction of **1d** with **MA**, the major product should be the 7-*exo* CA followed by the formation of the next significant 6-*exo* CA as these reaction channels are kinetically more favorable even though they are not thermodynamically more stable.

The thermodynamic parameters of the methyl substituted pyrazinium-3-olates **1b**–**d** with **MA** are gathered in Table S1. The activation enthalpy for the *exo* approach is lower compared to the *endo* approach and this is in agreement with the calculated activation energy. Additionally, a more negative activation entropy is observed for the *exo* channel than for the *endo* one. Consequently, the activation free energy for formation of the *exo* esters is lower than that for the *endo* esters. It can also be observed that the exothermicity decreases in the order **1b**>**1c**>**1d**.

3.2. Geometrical parameters

*3.2.1. 1,3-DC reactions of 1H-pyrazinium-3-olate **1** and 1-methylpyrazinium-3-olate **1a** with methyl acrylate.* The geometries of the TSs involved in the 1,3-DCs of the pyrazinium-3-olates **1** and **1a** with **MA** are presented in Figs. 1–3, Figs. S1 and S2. An analysis of the lengths of the two forming bonds at the TSs associated with these 1,3-DC reactions indicate that they are asynchronous concerted processes. At the regioisomeric TSs, the lengths of the C3–C2 and C3–C6 forming bonds are shorter than the C2–C6 and C2–C2 bonds, respectively. This suggests that the C–C bond formation at the more electrophilic conjugated C3 position of **MA** is more advanced than that at C2.

In the gas phase, the distance between the acidic *N*-hydrogen of the 1*H*-pyrazinium-3-olate and the carbonyl oxygen of **MA** at the most favorable **TS7ex-1** is 2.271 Å. This distance, which corresponds with an H–O hydrogen bond interaction at the TS, accounts for the large stabilization of **TS7ex-1** relative to **TS7en-1**; **TS7ex-1** is located 24.5 kJ mol^{-1} below **TS7en-1** (Table 1). However, this large stabilization found in the gas phase disappears in THF, and as

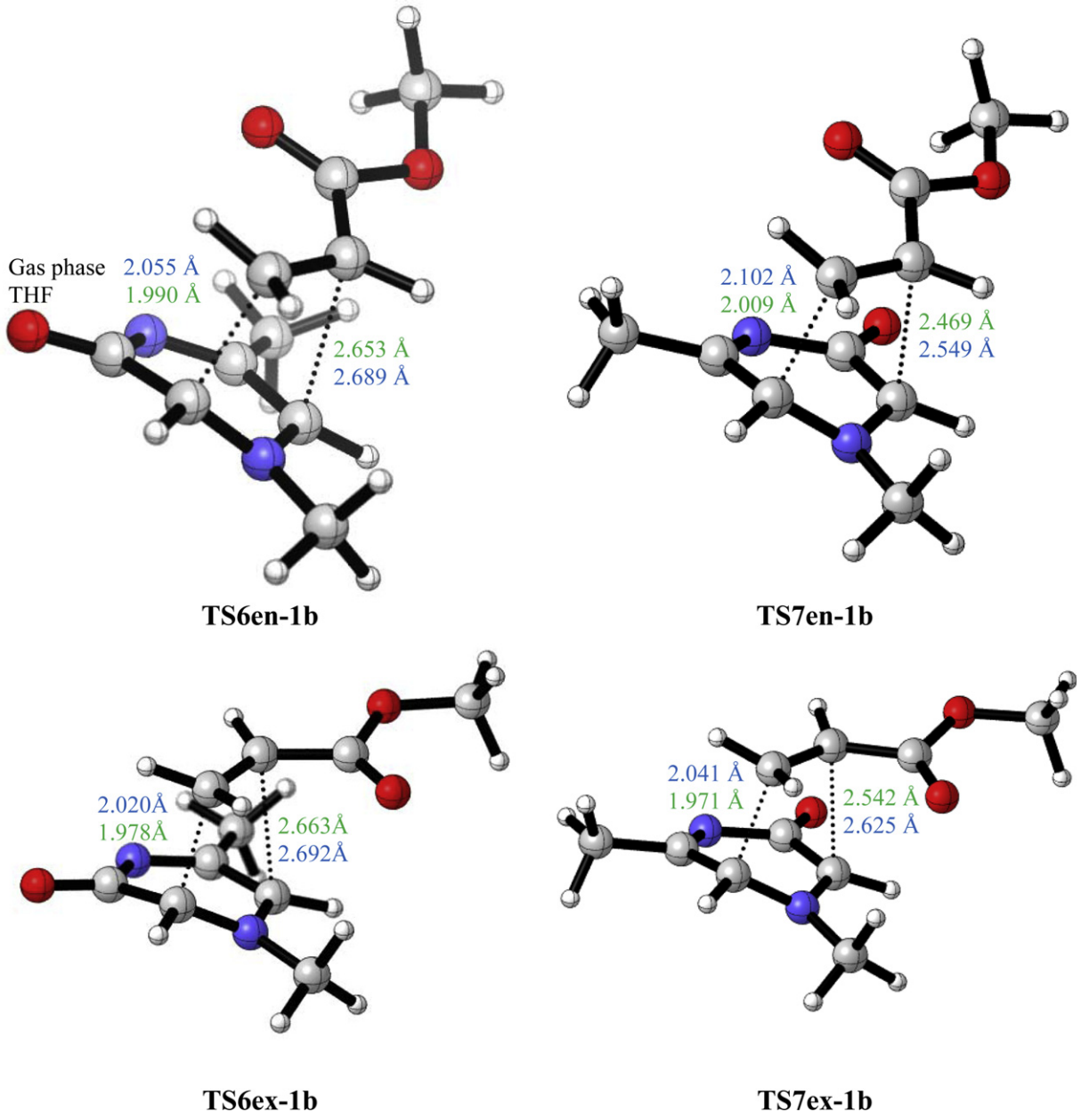

Fig. 3. B3LYP/6-31G(d) optimized geometries of the TSs involved in the 1,3-DC reaction between 1,5-dimethylpyrazinium-3-olate **1b** with **MA**.

a consequence, the energy difference between the two TSs decreases to 10.9 kJ mol^{-1}. Similarly, at **TS6ex-1** the distance of the H–O hydrogen bond is 2.318 Å, indicating a larger stabilization compared to **TS6en-1**. Once again, this stabilization is reduced in THF where a difference of 11.1 kJ mol^{-1} is observed. Inclusion of solvent effect causes a shortening of the forming bonds at C3 of **MA** in contrast to the forming bond length at C2, which increases. Thus, in THF, the TSs are slightly more advanced and show a higher degree of asynchronicity.

The asynchronicity of the TSs can be measured by considering the difference between the lengths of the two forming bonds such that $\Delta d_6=[d(\text{C2}-\text{C6})-d(\text{C3}-\text{C2})]$ for 6-ester pathways and $\Delta d_7=[d(\text{C2}-\text{C2})-d(\text{C3}-\text{C6})]$ for 7-ester pathways. Table 4 reports the degree of asynchronicity, Δd, of the TSs in both gas phase and THF. Overall TSs display varying degrees of asynchronicity when compared to the asynchronicity of the 1,3-DC reactions of 1*H*-pyridinium-3-olate and 1-methylpyridinium-3-olate with **MA**[38] where the *endo* TSs for the formation of the 6-esters are consistently more asynchronous than the *exo* TSs in the gas phase. In THF, however, greater asynchronicity is observed. Moreover, a comparison of the Δd for the reaction of **MA** with **1** and **1a** in the gas phase and in THF indicates that the Δd is larger with the pyrazinium-3-olate **1a** than with **1**. Conversely, the TSs for **1a** have higher Δd than the TSs of **1**, which correspond to the electron-releasing ability of the *N*-methyl group of **1a**. Thus, we can conclude that the presence of the methyl group leads to a more asynchronous *exo* TS. On comparing the asynchronicity of TSs for the 1,3-DC of pyridinium-3-olates and pyrazinium-3-olates with **MA**, it can be seen that the inclusion of a second nitrogen leads to more synchronous TSs.

3.2.2. Effect of adding a methyl substituent to pyrazinium-3-olate. The asynchronicity difference has also been calculated for the reaction of **1b**, **1c**, and **1d** with **MA**. Table S2 reports the asynchronicity degrees, Δd, in both the gas phase and in THF. A general trend observed is that the *exo* TSs are consistently more asynchronous relative to the *endo* TSs. Furthermore, the TSs leading to

Table 4
Δ*d* at the TSs arising from the 1,3-DC of **1** and **1a** with **MA**

	Δd_6		Δd_7
Gas phase			
TS6en-1	0.64 (0.74)[a]	**TS7en-1**	0.28 (0.36)[a]
TS6ex-1	0.58 (0.62)	**TS7ex-1**	0.35 (0.46)
TS6en-1a	0.65 (0.74)	**TS7en-1a**	0.31 (0.39)
TS6ex-1a	0.69 (0.72)	**TS7ex-1a**	0.51 (0.56)
THF			
TS6en-1	0.76 (0.90)	**TS7en-1**	0.50 (0.62)
TS6ex-1	0.63 (0.70)	**TS7ex-1**	0.44 (0.62)
TS6en-1a	0.77 (0.88)	**TS7en-1a**	0.55 (0.57)
TS6ex-1a	0.74 (0.78)	**TS7ex-1a**	0.66 (0.69)

[a] Values in parentheses are the asynchronicity for TSs involved in the 1,3-DC of 1*H*-pyridinium-3-olate and 1-methylpyridinium-3-olate with **MA** (see Ref. 38).

the 7-esters are more synchronous compared to the TSs leading to the 6-esters, with the **TS7en-1c** showing only a slight degree of asynchronicity. An exception is noted for the reaction of **1d** with **MA** in THF, where the *endo* **TS6en-1d** leading to the 6-esters presents a higher degree of asynchronicity relative to the *exo* **TS6ex-1d**. It is worthwhile pointing out that the asynchronicity difference is inversely proportional to the predicted activation energies.

3.3. Bond order and charge analysis

The Wiberg bond indices[74] have been computed to follow the nature of the cycloaddition process using NBO analysis. The bond order (BO) analysis of the TS arising from the 1,3-DC of 1*H*-pyrazinium-3-olate **1** and 1-methyl substituted pyrazinium-3-olates, **1a**–**d** with **MA** shows asynchronicity of the bond formation processes. The BO values of the two C–C forming bonds at the TSs for the cycloaddition of **1** and **1a** with **MA** are reported in Tables S3–S4. The BO values for the C3–C2 and C3–C6 bonds being formed at the regioisomeric TSs have larger values than the C2–C6 and C2–C2 bonds, respectively, in agreement with the predicted degree of asynchronicity. However, the polar character of the solvent increases the BO values of the C–C forming bond at the conjugated C3 of **MA**, and decreases the BO values of the C–C forming bond at C2, i.e., in solution the TSs are slightly more advanced and more asynchronous. It is noteworthy that the presence of a methyl group at the C6 position results in a low BO value for the C2–C6 bond formation process, indicating that the bond is partially formed due to the electron-donating ability of the methyl group.

The electronic nature of these 1,3-DC reactions is evaluated by analyzing the charge transfer (CT) at the TSs along the cycloaddition process. The natural atomic charges are shared between the pyrazinium-3-olate and **MA** fragments and these data are reported in Table 5. In the gas phase, the CT at the TSs, which fluxes from the pyrazinium-3-olate to the **MA** fragment, are in the range 0.09–0.20 e indicating some polar nature for these 1,3-DC reactions. For the more favorable *exo* TSs, the CT is slightly higher than for the *endo* ones. Moreover, in THF, the CT at the TSs slightly increases, a fact that is in agreement with a more advanced and more asynchronous character of the TSs.

Table 5
Charge transfer (CT, in e) and dipole moment (in Debye) of TSs

	1		**1a**		**1b**		**1c**		**1d**	
	CT	Dipole Moment	CT	Dipole Moment	CT	Dipole Moment	CT	Dipole Moment	CT	Dipole Moment
Gas phase										
TS6en	0.09	8.233	0.11	8.615	0.12	8.512	0.12	9.142	0.11	8.343
TS6ex	0.12	6.003	0.13	6.091	0.14	6.035	0.14	6.537	0.13	5.764
TS7en	0.10	7.394	0.11	7.818	0.13	7.753	0.11	8.046	0.14	7.834
TS7ex	0.14	5.174	0.16	5.664	0.17	5.775	0.15	5.939	0.20	5.723
THF										
TS6en	0.11	10.864	0.11	11.611	0.13	11.481	0.12	12.195	0.12	11.280
TS6ex	0.12	7.510	0.12	7.928	0.14	7.852	0.13	8.427	0.12	7.565
TS7en	0.15	9.976	0.15	10.651	0.16	10.627	0.13	10.674	0.18	10.737
TS7ex	0.15	6.717	0.18	7.745	0.18	7.978	0.16	7.894	0.21	7.842

Table 5 also reports the dipole moments of the TSs. The *endo* TSs are more polar than the *exo* TSs in spite of their larger CT. With the inclusion of solvent effect, the dipole moment of the TSs increases as a consequence of an increase of the CT. The greater polar character of the *endo* TSs than the *exo* TSs, measured by the dipole moments, accounts for the higher solvation of the former. This explains the changes in regioselectivity between the gas phase and the solvent results.

3.4. Analysis based on the global and local reactivity indexes at the ground state of reagents

Recent studies carried out on cycloaddition reactions[75–77] have shown that the analysis of the reactivity indices defined within the conceptual DFT[78,79] is a powerful tool to study the reactivity in polar cycloadditions. In Table 6, the static global properties (electronic chemical potential, μ, chemical hardness, η, global electrophilicity, ω, and global nucleophilicity, N) of pyrazinium-3-olates **1** and **1a**–**d**, and **MA** are presented.

Table 6
Electronic chemical potential, (μ, in eV), chemical hardness, (η, in eV), global electrophilicity, (ω, in eV), and global nucleophilicity, (N, in eV), of pyrazinium-3-olates **1** and **1a**–**d**, and **MA**

	μ	η	ω	N
1	−3.93	3.77	2.05	3.30
1a	−3.78	3.77	1.89	3.46
1c	−3.62	3.64	1.80	3.68
1b	−3.67	3.77	1.79	3.57
1d	−3.60	3.73	1.73	3.65
MA	−4.32	6.17	1.51	1.72

The electronic chemical potential of **MA**, μ=−4.32 eV, is lower than that for pyrazinium-3-olate **1**, μ=−3.93 eV, and for methyl substituted pyrazinium-3-olates, **1a**–**d**, $-3.78<\mu<-3.60$ eV, indicating thereby that along a polar cycloaddition reaction the net CT will take place from these pyrazinium-3-olates towards the electron-deficient **MA**.

Pyrazinium-3-olate **1** presents both high electrophilicity, ω=2.05 eV, and high nucleophilicity, N=3.30 eV, being classified both as strong electrophile and strong nucleophile within the electrophilicity[75] and nucleophilicity[80] scales. Methyl substituted pyrazinium-3-olates **1a**–**d** present electrophilicity indices between $1.89<\omega<1.73$ eV, and nucleophilicity indices between $3.46<N<3.68$ eV, being classified also as strong electrophiles and strong nucleophiles. Inclusion of one or two electron-releasing methyl groups on pyrazinium-3-olate **1** both decreases the electrophilicity and increases the nucleophilicity of methyl derivatives **1a**–**d**.

Pyridinium-3-olates present electrophilicity indices of ω=1.43 eV (**R**=**H**) and ω=1.36 eV (**R**=**Me**),[38] being classified as moderate electrophiles, and nucleophilicity indices of N=3.91 eV (**R**=**H**) and N=4.02 eV (**R**=**Me**), being classified as strong nucleophiles. Therefore, the inclusion of a second nitrogen atom in the pyridinium-3-olates, increases the electrophilicity and decreases the nucleophilicity of the pyrazinium-3-olates **1a**–**d**.

MA has an electrophilicity index of ω=1.51 eV, at the borderline of the strong electrophiles, and a nucleophilicity index of N=1.72 eV, being classified as a marginal nucleophile. Consequently, **MA** is a poorer electrophile than pyrazinium-3-olates **1** and **1a**–**d**.

Based on the analysis of the electrophilicity indices, it is expected that in a polar cycloaddition, pyrazinium-3-olates **1** and

1a–**d** will act as electrophiles while **MA** will act as nucleophile. However, analysis of the electronic chemical potential of these compounds indicates that in a polar process the net CT will take place from pyrazinium-3-olates **1** and **1a**–**d** to **MA**. On the other hand, pyrazinium-3-olates **1** and **1a**–**d** are strong nucleophiles, while **MA** is a marginal nucleophile. Therefore, along electrophilic/nucleophilic interactions, the more favorable ones will be between **MA** acting as electrophile and pyrazinium-3-olates **1** and **1a**–**d** acting as nucleophiles. These behaviors are in agreement with the analysis of the CT performed at the corresponding TSs, which fluxes from **1** and **1a**–**d** toward **MA**. On the other hand, the low CT found at the TSs, less than 0.20 e, is a consequence of the low electrophilicity of **MA**.

The local electrophilicity ω_k of **MA** and the local nucleophilicity N_k of the pyridinium-3-olates **1** and **1a**–**d** were analyzed in order to predict the best electrophilic/nucleophilic interaction and, therefore, to explain the observed regioselectivity (see Table 7). When **MA** behaves as an electrophile, the most electrophilic site is the conjugated C3 position, ω_k=0.62 eV.[38] Finally, analysis of the local nucleophilicity N_k at pyrazinium-3-olates **1** and **1a**–**d** indicates that the relative position of the methyl groups on the pyrazinium ring does not have a significant influence on the regioselectivity of polar reactions, it being controlled by the relative position of the two nitrogen atoms compared to the nucleophilic oxygen atom.

Table 7
Local nucleophilicity (Nk, in eV) indices of pyrazinium-3-olates **1** and **1a**–**d**

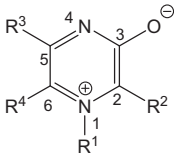

	1	1a	1b	1c	1d
N1	0.02	0.02	0.02	0.02	0.02
C2	0.73	0.73	0.76	0.79	0.71
C3	0.03	0.03	0.03	0.03	0.04
N4	0.52	0.57	0.60	0.52	0.60
C5	0.02	0.02	0.02	0.04	0.04
C6	0.90	0.96	1.03	0.89	1.02
O	1.09	1.12	1.20	1.15	1.14

Analysis of the local nucleophilicity N_k at the six positions of the pyrazinium-3-olate ring indicates that the C2 and C6 carbons are the more nucleophilically activated positions. The C6 position is more activated than the C2, indicating that the more favorable polar reaction will take place by the nucleophilic attack of the C6 position of pyrazinium-3-olate to the conjugated C3 position of **MA**, allowing the formation of the 7-regioisomeric CAs. Although this analysis does not agree entirely with the energy results, it is interesting to note that the CTs at the 7-regioisomeric TSs are slightly larger than that at the 6-regioisomers (see Table 5).

3.5. Rate constants

The rate constant for the second order elementary step, k_1 and the effective rate constant, k_{ef}, for the 1,3-DC of the substituted pyrazinium-3-olates with **MA** are reported in Table S5. An analysis of the rate constants from Table S5 indicates that firstly the *exo* channel has a larger rate constant than the *endo* channel whereby the 6-*exo* and 6-*endo* pathways are the faster reaction channels compared to the 7-*exo* and 7-*endo* pathways, respectively. Secondly, there is a good agreement with the values of the k_1 calculated from Eq. 3 and 6. Thirdly, on comparing the 1,3-DC of pyridinium-3-olates and pyrazinium-3-olates with **MA**, it is found that the larger rate constants, k_1, are associated with the pyrazinium-3-olates. In general the variations in the rate constants can be rationalized in terms of activation energies.

4. Conclusions

DFT computations using B3LYP functional in conjunction with the 6-31G(d) basis set have been used to analyze the outcome of the 1,3-DC reactions of 1*H*-pyrazinium-3-olate and *N*1- and *C*-methyl substituted pyrazinium-3-olates with **MA**. Solvent effects of THF were also evaluated so as to mimic the experimental environment and it was found that reliable results were obtained in solvent phase which favors the same regiochemical sense as literature experimental outcomes. Thermodynamic and kinetic parameters of the possible *endo*/*exo* stereoisomeric and 6-ester/7-ester regioisomeric pathways have been determined. The rate constants of the second order elementary step were calculated at room temperature using conventional TST. The 1,3-DC of 1,5-dimethylpyrazinium-3-olate that we reported[27,31] is consistent with the theoretical results where the 6-*exo* CA is formed as the major product; the activation energies favor the formation of the 6-*exo* over the 6-*endo* by 7.8 kJ mol^{-1}. Related systems, which are experimentally untried, were studied so as to predict the effect of varying the position of the methyl group on the pyrazinium-3-olate ring. It is found that the formation of 6-esters is preferred over the 7-esters where the reaction channel leading to the 6-*exo* CA is preferred. On comparing the 1,3-DC of pyridinium-3-olates and pyrazinium-3-olates with **MA**, it is found that lower activation energies and more stable CAs are formed with the inclusion of a second nitrogen as in the pyrazinium-3-olates. Further, more advanced and synchronous TSs are observed with pyrazinium-3-olates. The outcome of this research provides incentive to study the 1,3-DC of more hindered pyrazinium-3-olates with **MA** and methyl methacrylate so as to take into account the effect of adding more methyl groups to the system. This will be the subject of a future communication.

Acknowledgements

The authors acknowledge comments from anonymous reviewers. Facilities from the Universiti Sains Malaysia and University of Mauritius are acknowledged. This work was supported by funding provided by the Mauritius Tertiary Education Commission (TEC). L.R.D. acknowledges research funds provided by the Ministerio de Ciencia e Innovación of the Spanish Government (project CTQ2009-11027/BQU).

Supplementary data

Supplementary data associated with this article can be found, in the online version, at doi:10.1016/j.tet.2011.08.021.

References and notes

1. Huisgen, R. *Angew. Chem., Int. Ed. Engl.* **1963**, *2*, 565–598.
2. Padwa, A. In *1,3-Dipolar Cycloaddition Chemistry*; Wiley-Interscience: New York, NY, 1984; Vol. 1–2.
3. Namboothiri, I. N. N.; Rastogi, N.; Ganguly, B.; Mobin, S. M.; Cojocaru, M. *Tetrahedron* **2004**, *60*, 1453–1462.
4. Pandey, G.; Banerjee, P.; Gadre, S. R. *Chem. Rev.* **2006**, *106*, 4484–4517.
5. Nair, V.; Suja, T. D. *Tetrahedron* **2007**, *63*, 12247–12275.
6. Pellissier, H. *Tetrahedron* **2007**, *63*, 3235–3285.
7. Saubern, S.; Macdonald, J. M.; Ryan, J. H.; Woodgate, R. C. J.; Louie, T. S.; Fuchter, M. J.; White, J. M.; Holmes, A. B. *Tetrahedron* **2010**, *66*, 2761–2767.
8. Feng, G.-L.; Zhang, H.-L.; Geng, J.-L. *J. Chem. Res.* **2011**, *35*, 121–123.
9. Danielsson, J.; Toom, L.; Somfai, P. *Eur. J. Org. Chem.* **2011**, *2011*, 607–613.
10. Nonn, M.; Kiss, L.; Forró, E.; Mucsi, Z.; Fülöp, F. *Tetrahedron* **2011**, *67*, 4079–4085.

11. Padwa, A. In *Synthetic Applications of 1,3-Dipolar Cycloaddition Chemistry Toward Heterocycles and Natural Products*; Padwa, A., Pearson, W. H., Eds.; Wiley: Hoboken, 2003.
12. Merino, P. In *Science of Synthesis*; Padwa, A., Ed.; George Thieme: New York, NY, 2004; Vol. 27, pp 511–580.
13. Desimoni, G.; Tacconi, G.; Barco, A.; Pollini, G. P. In *Natural Products Synthesis through Pericyclic Reactions*; American Chemical Society: Washington, 1983.
14. Massiot, G.; Delaude, C. *The Alkaloids* **1986**, *27*, 300–321.
15. Plunkett, A. O. *Nat. Prod. Rep.* **1994**, *11*, 581–590.
16. Chorghade, M. S.; Cseke, C. *Pure Appl. Chem.* **1994**, *66*, 2211–2214.
17. Kaval, N.; Ermolat'ev, D.; Appukkuttan, P.; Dehaen, W.; Kappe, C. O.; Van der Eycken, E. *J. Comb. Chem.* **2005**, *7*, 490–502.
18. Pawar, V.; De Borggraeve, W. M. *Synthesis* **2006**, *17*, 2799–2814.
19. Samorí, C.; Ali-Boucetta, H.; Sainz, R.; Guo, C.; Toma, F. M.; Fabbro, C.; da Ros, T.; Prato, M.; Kostarelos, K.; Bianco, A. *Chem. Commun.* **2010**, *46*, 1494–1496.
20. Hashimoto, T.; Maeda, Y.; Omote, M.; Nakatsu, H.; Maruoka, K. *J. Am. Chem. Soc.* **2010**, *132*, 4076–4077.
21. Katritzky, A. R.; Takeuchi, Y. *J. Chem. Soc. C* **1971**, 874–877.
22. Dennis, N.; Katritzky, A. R.; Matsuo, T.; Parton, S. K. *J. Chem. Soc., Perkin Trans. 1* **1973**, 746–750.
23. Banerji, J.; Dennis, N.; Frank, J.; Katritzky, A. R. *J. Chem. Soc., Perkin Trans. 1* **1975**, 2334–2338.
24. Dennis, N.; Katritzky, A. R.; Takeuchi, Y. *Angew. Chem., Int. Ed. Engl.* **1976**, *15*, 1–9.
25. Katritzky, A. R.; Dennis, N. *Chem. Rev.* **1989**, *89*, 827–861.
26. Allway, P. A.; Sutherland, J. K.; Joule, J. A. *Tetrahedron Lett.* **1990**, *31*, 4781–4783.
27. Yates, N. D.; Peters, D. A.; Beddoes, R. L.; Scopes, D. I. C.; Joule, J. A. *Heterocycles* **1995**, *40*, 331–347.
28. Helliwell, M.; You, Y.; Joule, J. A. *Acta Crystallogr., Sect. E: Struct. Rep. Online* **2006**, *E62*, o1293–o1294.
29. Helliwell, M.; You, Y.; Joule, J. A. *Acta Crystallogr., Sect. E: Struct. Rep. Online* **2006**, *E62*, o2318–o2320.
30. Helliwell, M.; Yun, Y.; Joule, J. A. *Heterocycles* **2006**, *70*, 87–91.
31. Kiss, M.; Russell-Maynard, J.; Joule, J. A. *Tetrahedron Lett.* **1987**, *28*, 2187–2190.
32. Joomun, Z.; Raftery, J.; Delawarally, K.; Jhaumeer-Laulloo, S.; Joule, J. A. *Arkivoc* **2007**, *xvi*, 51–57.
33. Türker, L.; Gümüş, S. *J. Comput. Theor. Nanosci.* **2009**, *6*, 873–879.
34. Benchouk, W.; Mekelleche, S. M.; Aurell, M. J.; Domingo, L. R. *Tetrahedron* **2009**, *65*, 4644–4651.
35. Xu, L.; Doubleday, C. E.; Houk, K. N. *J. Am. Chem. Soc.* **2010**, *132*, 3029–3037.
36. Domingo, L. R.; Sáez, J. A. *J. Org. Chem.* **2011**, *76*, 373–379.
37. La Porta, F. A.; Ramalho, T. C.; Santiago, R. T.; Rocha, M. V. J.; da Cunha, E. F. F. *J. Phys. Chem. A* **2011**, *115*, 824–833.
38. Rhyman, L.; Abdallah, H. H.; Jhaumeer-Laulloo, S.; Domingo, L. R.; Joule, J. A.; Ramasami, P. *Tetrahedron* **2010**, *66*, 9187–9193.
39. Guiheneuf, G.; Laurence, C.; Katritzky, A. R. *J. Chem. Soc., Perkin Trans. 2* **1976**, 1829–1831.
40. Takahashi, K.; Tomita, F. *J. Antibiot.* **1983**, *36*, 468–470.
41. Tomita, F.; Takahashi, K.; Shimizu, K. *J. Antibiot.* **1983**, *36*, 463–467.
42. Hirayama, N.; Shirahata, K. *J. Chem. Soc., Perkin Trans. 2* **1983**, 1705–1708.
43. He, H.; Shen, B.; Carter, G. T. *Tetrahedron Lett.* **2000**, *41*, 2067–2071.
44. Frisch, M. J.; Trucks, G. W.; Schlegel, H. B.; Scuseria, G. E.; Robb, M. A.; Cheeseman, J. R.; Montgomery, J. A., Jr.; Vreven, T.; Kudin, K. N.; Burant, J. C.; Millam, J. M.; Iyengar, S. S.; Tomasi, J.; Barone, V.; Mennucci, B.; Cossi, M.; Scalmani, G.; Rega, N.; Petersson, G. A.; Nakatsuji, H.; Hada, M.; Ehara, M.; Toyota, K.; Fukuda, R.; Hasegawa, J.; Ishida, M.; Nakajima, T.; Honda, Y.; Kitao, O.; Nakai, H.; Klene, M.; Li, X.; Knox, J. E.; Hratchian, H. P.; Cross, J. B.; Bakken, V.; Adamo, C.; Jaramillo, J.; Gomperts, R.; Stratmann, R. E.; Yazyev, O.; Austin, A. J.; Cammi, R.; Pomelli, C.; Ochterski, J. W.; Ayala, P. Y.; Morokuma, K.; Voth, G. A.; Salvador, P.; Dannenberg, J. J.; Zakrzewski, V. G.; Dapprich, S.; Daniels, A. D.; Strain, M. C.; Farkas, O.; Malick, D. K.; Rabuck, A. D.; Raghavachari, K.; Foresman, J. B.; Ortiz, J. V.; Cui, Q.; Baboul, A. G.; Clifford, S.; Cioslowski, J.; Stefanov, B. B.; Liu, G.; Liashenko, A.; Piskorz, P.; Komaromi, I.; Martin, R. L.; Fox, D. J.; Keith, T.; Al-Laham, M. A.; Peng, C. Y.; Nanayakkara, A.; Challacombe, M.; Gill, P. M. W.; Johnson, B.; Chen, W.; Wong, M. W.; Gonzalez, C.; Pople, J. A. *Gaussian 03, Revision B.03*; Gaussian: Wallingford CT, 2004.
45. Becke, A. D. *J. Chem. Phys.* **1988**, *38*, 3098–3100.
46. Lee, C.; Yang, W.; Parr, R. G. *Phys. Rev. B* **1988**, *37*, 785–789.
47. Hehre, W. J.; Radom, L.; Schleyer, P. v. R.; Pople, J. A. *Ab Initio Molecular Orbital Theory*; Wiley: New York, NY, 1986.
48. Goldstein, E.; Beno, B.; Houk, K. N. *J. Am. Chem. Soc.* **1996**, *118*, 6036–6043.
49. Domingo, L. R.; Arnó, M.; Andrés, J. *J. Am. Chem. Soc.* **1998**, *120*, 1617–1618.
50. Garcia, J. I.; Martinéz-Merino, V.; Mayoral, J. A.; Salvatella, L. *J. Am. Chem. Soc.* **1998**, *120*, 2415–2420.
51. CYLview, 1.0b Legault, C. Y. *Université de Sherbrooke*; 2009;; http://www.cylview.org.
52. Gonzalez, C.; Schlegel, H. B. *J. Chem. Phys.* **1989**, *90*, 2154–2161.
53. Gonzalez, C.; Schlegel, H. B. *J. Phys. Chem.* **1990**, *94*, 5523–5527.
54. Cances, M. T.; Mennunci, V.; Tomasi, J. *J. Chem. Phys.* **1997**, *107*, 3032–3041.
55. Cossi, M.; Baronne, V.; Cammi, R.; Tomasi, J. *Chem. Phys. Lett.* **1996**, *255*, 327–355.
56. Barone, V.; Cossi, M.; Tomasi, J. *J. Comput. Chem.* **1998**, *19*, 404–417.
57. Tomasi, J.; Persico, M. *Chem. Rev.* **1994**, *94*, 2027–2094.
58. Simkin, B. Y.; Sheikhet, I. In *Quantum Chemical and Statistical Theory of Solutions—A Computational Approach*; Ellis Horwood: London, 1995.
59. Scott, A. P.; Radom, L. *J. Phys. Chem.* **1996**, *100*, 16502–16513.
60. Reed, A. E.; Weinstock, R. B.; Weinhold, F. *J. Chem. Phys.* **1985**, *83*, 735–746.
61. Reed, A. E.; Curtiss, L. A.; Weinhold, F. *Chem. Rev.* **1988**, *88*, 899–926.
62. Parr, R. G.; von Szentpaly, L.; Liu, S. *J. Am. Chem. Soc.* **1999**, *121*, 1922–1924.
63. Parr, R. G.; Pearson, R. G. *J. Am. Chem. Soc.* **1983**, *105*, 7512–7516.
64. Parr, R. G.; Yang, W. In *Density Functional Theory of Atoms and Molecules*; Oxford University: New York, NY, 1989.
65. Kohn, W.; Sham, L. *J. Phys. Rev. A* **1965**, *140*, 1133–1138.
66. Domingo, L. R.; Chamorro, E.; Pérez, P. *J. Org. Chem.* **2008**, *112*, 4615–4624.
67. Domingo, L. R.; Aurell, M. J.; Pérez, P.; Contreras, R. *J. Phys. Chem. A* **2002**, *106*, 6871–6875.
68. Pérez, P.; Domingo, L. R.; Duque-Noreña, M.; Chamorro, E. *J. Mol. Struct. (THEOCHEM)* **2009**, *895*, 86–91.
69. Contreras, R.; Fuentealba, P.; Galván, M.; Pérez, P. *Chem. Phys. Lett.* **1999**, *304*, 405–413.
70. Truhlar, D. G.; Issacson, A. D.; Garett, B. C. In *Generalized Transition State Theory Theory of Chemical Reaction Dynamics*; CRC: Boca Raton, Florida, 1985; Vol. 4, pp 65–137.
71. Pilling, M. J.; Seakins, P. W. In *Reaction Kinetics Oxford Science: Oxford, 1995.*
72. Barreto, P. R. P.; Vilela, A. F. A.; Gargano, R. *Int. J. Quantum Chem.* **2005**, *103*, 685–694.
73. Wigner, E. P. *Z. Phys. Chem. B* **1932**, *19*, 203–216.
74. Wiberg, K. B. *Tetrahedron* **1968**, *24*, 1083–1096.
75. Domingo, L. R.; Aurell, M. J.; Pérez, P.; Contreras, R. *Tetrahedron* **2002**, *58*, 4417–4423.
76. Pérez, P.; Domingo, L. R.; Aurell, M. J.; Contreras, R. *Tetrahedron* **2003**, *59*, 3117–3125.
77. Pérez, P.; Domingo, L. R.; Aizman, A.; Contreras, R. In *Theoretical Aspects of Chemical Reactivity*; Toro-Labbé, A., Ed.; Elsevier Science: Amsterdam, the Netherlands, 2007; Vol. 19, pp 139–201.
78. Geerlings, P.; De Proft, F.; Langenaeker, W. *Chem. Rev.* **2003**, *103*, 1793–1873.
79. Ess, D. H.; Jones, G. O.; Houk, K. N. *Adv. Synth. Catal.* **2006**, *348*, 2337–2361.
80. Jaramillo, P.; Domingo, L. R.; Chamorro, E.; Pérez, P. *J. Mol. Struct. THEOCHEM* **2008**, *865*, 68–72.